



HAL
open science

Experimental and kinetic modeling study of n-hexane oxidation. Detection of complex low-temperature products using high-resolution mass spectrometry

Nesrine Belhadj, Maxence Lailliau, Roland Benoit, Philippe Dagaut

► To cite this version:

Nesrine Belhadj, Maxence Lailliau, Roland Benoit, Philippe Dagaut. Experimental and kinetic modeling study of n-hexane oxidation. Detection of complex low-temperature products using high-resolution mass spectrometry. *Combustion and Flame*, 2021, 233, pp.111581. 10.1016/j.combustflame.2021.111581 . hal-03291957

HAL Id: hal-03291957

<https://hal.science/hal-03291957v1>

Submitted on 20 Jul 2021

HAL is a multi-disciplinary open access archive for the deposit and dissemination of scientific research documents, whether they are published or not. The documents may come from teaching and research institutions in France or abroad, or from public or private research centers.

L'archive ouverte pluridisciplinaire **HAL**, est destinée au dépôt et à la diffusion de documents scientifiques de niveau recherche, publiés ou non, émanant des établissements d'enseignement et de recherche français ou étrangers, des laboratoires publics ou privés.

Copyright

Experimental and kinetic modeling study of n-hexane oxidation. Detection of complex low-temperature products using high-resolution mass spectrometry.

Nesrine Belhadj^{1,2}, Maxence Lailliau^{1,2}, Roland Benoit¹, Philippe Dagaut^{1,*}

¹ CNRS–INSIS, ICARE, 1C avenue de la Recherche Scientifique, 45071 Orléans cedex 2, France

² Université d'Orléans, rue de Chartres, 45100 Orléans, France

*Corresponding author:

Philippe Dagaut

CNRS–ICARE, Institut de Combustion, Aérothermique, Réactivité et Environnement

1C Avenue de la Recherche Scientifique

45071 Orléans Cedex 2, France

Tel: +33 (0)2 38 25 54 66

dagaut@cnrs-orleans.fr

Abstract

This study concerns the oxidation of n-hexane. It was conducted in continuous flow fused-silica jet-stirred reactor (JSR) at 10 atm and an equivalence ratio of 0.5. n-Hexane initial concentrations were (i) 2500 ppm with a mean residence time of 1.5 s and (ii) 1000 ppm with a mean residence time of 0.7 s; we operated in the cool-flame regime for temperatures ranging from 540 to 720K and 530 to 800K, respectively. Products were analyzed and quantified in the gas phase using gas chromatography (with flame ionization, thermal conductivity, and quadrupole mass spectrometry) and Fourier transform infrared spectrometry. Products of low-temperature oxidation were sampled in the JSR and trapped in acetonitrile for characterization using an Orbitrap Q-Exactive®. Flow injection analyses (FIA) and ultra-high pressure liquid chromatography (UHPLC) coupled with atmospheric pressure chemical ionization (APCI +/- modes)- high resolution mass spectrometry (HRMS) analyses were used to characterize hydroperoxides (C₆H₁₄O₂), keto-hydroperoxides (C₆H₁₂O₃, C₃H₆O₃, C₄H₈O₃, and C₅H₁₀O₃), cyclic ethers (C₆H₁₂O), carboxylic acids (C₂ to C₆), ketones (C₃ to C₆), diones (C₆H₁₀O₂), unsaturated ketones (C₆H₁₀O and C₆H₈O), unsaturated diones (C₆H₈O₂), and highly oxygenated molecules (C₆H₁₂O₄₋₈) produced by addition of three and four oxygen molecules on fuel's radicals. To confirm the presence of hydroxyl or hydroperoxyl groups in the oxidation products we used H/D exchange with D₂O. 2,4-Dinitrophenylhydrazine (2,4-DNPH) derivatization was used to characterize and confirm the presence of different carbonyls which can be formed during the low temperature oxidation of n-hexane. An available kinetic reaction mechanism including 3rd O₂ addition on fuel's radicals was used to simulate the formation of the presently detected keto-hydroperoxides (KHP) and highly oxygenated molecules (HOMs).

Keywords: n-hexane, cool flame, keto-hydroperoxides, highly oxygenated molecules, Orbitrap, jet-stirred reactor

1. Introduction

Normal and branched alkanes are major constituents of commercial liquid fuels [1-3]. Recently, n-alkanes such as n-hexane have been used as additives to conventional fuels for improving the combustion properties and efficiency of diesel engines [4-6]. The ignition, combustion, and oxidation of primary reference fuels has already been the topic of many studies conducted over a wide range of conditions. Techniques such as shock tubes, rapid compression machines, burners, combustion chambers, reactors, and piston engines have been used. In comparison, the oxidation of intermediate length alkanes such as n-hexane has received less attention. Previous studies have focused mainly on the high-temperature oxidation of n-hexane, while few studies have been conducted under low-temperature oxidation regime. Burcat et al. have reported ignition delay times for n-hexane-O₂-Ar mixtures in a shock tube over a range of temperatures (1020–1725 K) and pressures (1–7 atm) [7]. Zhukov et al. have determined ignition delay times for n-hexane over an higher range of pressures (~11–244 atm) and still high-temperatures (822–1380 K) [8]. Mével et al. [9] have studied the atmospheric pressure oxidation of n-hexane in a flow reactor at low temperatures (450–1000 K). More recently, Wang et al. [10] have reported a study of the atmospheric pressure oxidation of the five hexane isomers at low-temperature (550–1000 K) in a JSR. They have measured intermediates and products concentrations by both gas chromatography and synchrotron-based mass spectrometry [11]. Cyclic ether isomers mainly formed in the NTC region have been identified and quantified. At the same time, Zhang et al. [12] have reported an extensive set of experimental data for n-hexane oxidation: ignition delay times of stoichiometric n-hexane mixtures in synthetic air (21% O₂ and 79% diluent) determined using a rapid compression machine and a shock tube (627–1365 K, 15–32 bar), and speciation in a JSR (530–1160 K, 10 atm). These data

were used by Zhang et al. [13] to update a detailed kinetic reaction mechanism for n-hexane oxidation. Later, Wang and Sarathy [14] extended the model of Zhang et al. [13] by introducing the third addition of molecular oxygen on fuel's radicals. Nevertheless, under piston engines operating conditions, i.e., low-temperature and high-pressure conditions, there is a lack of data for the complex pool of intermediates governing ignition and pollutants formation [15]. Relatively few studies have reported the formation of elusive low-temperature oxidation products, e.g. fuel's hydroperoxides (ROOH), keto-hydroperoxides (KHPs) [16-24], and highly oxygenated molecules (HOMs). Such species were recently observed in oxidation experiments involving a JSR and Molecular beam- synchrotron-vacuum UV-Photoionization-TOF MS and/or HESI- or APCI-Orbitrap® (heated electrospray ionization, atmospheric pressure chemical ionization), conducted for a range of fuels [15, 25-34]. Besides the autoxidation route considered in combustion yielding ketohydroperoxides, i.e., $\text{fuel} + \text{X}^{\bullet} (\text{OH}, \text{H}^{\bullet}, \text{O}^{\bullet}, \text{HO}_2^{\bullet}, \text{O}_2 \dots) \rightarrow \text{R}^{\bullet} + \text{XH}$; $\text{R} + \text{O}_2 \rightarrow \text{ROO}^{\bullet} \rightarrow \text{QOOH}$ (H-shift); $\text{QOOH} + \text{O}_2 \rightarrow \text{OOQOOH} \rightarrow \text{HOOQ}=\text{O} + \text{OH}^{\bullet}$, a pathway involving peroxy radicals' self-reaction, considered in atmospheric chemistry but neglected in combustion, can play a role, i.e., $2 \text{ROO}^{\bullet} \rightarrow \text{ROOOOR} \rightarrow 2 \text{RO}^{\bullet} + \text{O}_2$; $\text{RO}^{\bullet} \rightarrow \text{QOH}$ (H-shift); $\text{QOH} + \text{O}_2 \rightarrow \text{OOQOH} \rightarrow \text{OQ}^{\bullet}\text{OH} + \text{OH}^{\bullet}$.

HOMs formation is usually ignored in combustion while they represent major intermediates for the formation of secondary organic aerosols in the atmosphere [35]. The separation of KHPs formed by oxidation of large hydrocarbons has been pursued using chromatography and detection by UV absorption or mass spectrometry [16-24], but until recently the authors faced technical limitations. With recent powerful analytical techniques such as ultra-high pressure liquid chromatography (UHPLC), and high-resolution mass spectrometry (Orbitrap®) one can improve the characterization of complex low-temperature oxidation products [29, 31-34, 36].

As part of ongoing efforts for increasing our knowledge of fuels' cool-flame oxidation mechanisms, a series of experiments were conducted in a JSR. They aim to better characterizing the low temperature oxidation products of n-hexane. To this end, gas chromatography (GC), Fourier Transform Infrared spectrometry (FTIR), liquid chromatography (UHPLC) and Orbitrap were used. Hydroperoxides, unsaturated hydroperoxides, keto-hydroperoxides, diones, ketones, aldehydes, carboxylic acids, cyclic ethers, and extensively oxygenated molecules, formed via multiple O_2 additions on fuel's radicals and H-shifts, were detected using soft chemical ionization (APCI +/-) and high-resolution mass spectrometry (HRMS). A chemical kinetic scheme involving HOMs formation routes [14] was tested against the present data.

2. Experimental

2.1 Experiments in a JSR

We conducted experiments in a JSR described earlier [37] and used in previous works addressing the kinetics of oxidation of gas and liquid fuels, e.g., [38-40]. The JSR is located inside a temperature-controlled oven (ca. 1.5 kW), which maintains the reactor at the desired working temperature, surrounded by insulating ceramic wool and a pressure-resistant stainless-steel housing. The temperature of the JSR was varied stepwise. As before [41] n-hexane (>99% pure from Sigma Aldrich) was atomized and vaporized using an in-house setup. The fuel- N_2 and O_2 - N_2 mixtures flowed separately to the four JSR injectors (nozzles of 1 mm I.D.) to avoid premature fuel oxidation. N_2 and O_2 flow rates were controlled by mass flow meters (Brooks). n-Hexane was pumped by means of an HPLC pump (Shimadzu LC10 AD VP) equipped with an online degasser (Shimadzu DGU-20 A3). Table 1 gives the experimental conditions. To better probe the formation of highly oxygenated products, besides operating with 1000 ppm of n-hexane, as in our earlier works, we performed experiments with higher fuel concentrations (2500 ppm).

Table 1. Experimental conditions.

	Condition 1	Condition 2
Initial fuel, O_2 , and N_2 concentration	2500 ppm, 4.75 %, 95 %	1000 ppm, 1.9 %, 98%
Equivalence ratio (ϕ)	0.5	0.5
Residence time	1.5 s	0.7 s
Pressure	10 atm	10 atm
Temperature range	540 to 720 K	530 to 800 K

Pt-Pt/Rh-10% thermocouples (wires of 100 μm insulated inside a thin-wall fused-silica housing) were used to check thermal homogeneity throughout the vertical axis of the reactor. Gradients of < 1 K/cm were measured. A movable low-pressure fused-silica sonic probe was used to take samples for analyses. Products were analyzed in

the gas phase by GC (with flame ionization-FID, thermal conductivity-TCD, and quadrupole mass spectrometry) and online FTIR. External calibration was used for quantifications.

Cool-flame products, e.g., hydroperoxides, cyclic ethers, keto-hydroperoxides (KHPs), di-keto-hydroperoxides, keto-di-hydroperoxides, and other highly oxygenated products were also measured. Gas samples exiting the sonic probe were directed to an amber glass vial filled with acetonitrile for 75 min (0°C, 25 mL). The sample solutions were stored at -15°C in a freezer for future chemical analyses.

2.2 Orbitrap analyses

We followed the procedure described in recent publications [29, 32, 42-45]. Oxidized products were analyzed by gas chromatography and reverse-phase liquid chromatography (Table 2). HRMS analyses were conducted by flow injection (FIA). The liquid samples were injected into the APCI chamber of an Orbitrap® Q-Exactive mass spectrometer (resolution $m/\Delta m = 140,000$ at m/z 200; mass accuracy < 1 ppm RMS). The instrument allows for ‘exact mass’ measurements, not attainable with other techniques such as Q-ToF or time-of-flight MS (mass resolution ca. 4000). Also, UHPLC-HRMS (Thermo Scientific) was used. Soft ionization of samples was done using an Ion Max® atmospheric pressure chemical ionization (APCI) in positive and negative modes (Table 3). This technique is suitable for the detection of moderate polarity compounds, such as the products of low-temperature oxidation of n-hexane. MS-MS analyses were conducted at higher energy collisional dissociation (HCD) of 10 eV in order to determine the chemical structure of products based on their fragments.

Table 2. Gas-phase chromatography and reverse-phase liquid chromatography analyses conditions.

	GC	UHPLC
Analytical column	Coupling of two capillary columns: CP-Sil 5CB (1.2 μm , 0.32 mm, 25m) and DB-1 (3 μm , 0.53 mm, 30m)	C ₁₈ (Phenomenex Luna, 1.6 μm , 100 Å, 100x2.1 mm)
Oven temperature	Constant at 35°C for 30 min, increasing by 1°C/min until 60°C, increased by 10°C/min until 200°C. keep 200°C for 1 min.	40°C
Carrier gas mobile phase	(1) Helium and (2) nitrogen Flow rate (1) 1.5 ml/min and (2) 15 mL/min	Water/Acetonitrile Elution gradient: 3 to 100% ACN. Flow rate 250 $\mu\text{l}/\text{min}$
Analysis duration	(1) 70 min and (2) 1.5 min	18 min
Detector	(1) FID, MS (quadrupole), (2) TCD	HRMS (Orbitrap)

Table 3. APCI settings during FIA and UHPLC-MS analyses

	FIA	UHPLC
Syringe or mobile phase flow rate ($\mu\text{l}/\text{min}$)	3 to 5	250
Sheath gas flow (a.u)	10	50
Auxiliary gas flow (a.u)	1	10
Sweep gas flow (a.u)	0	0
Capillary temperature (°C)	150	150
Vaporizer temperature (°C)	100	150
Corona discharge current (μA)	4 to 5	4 to 5
Spray voltage (kV)	4.2	4.2

To verify the presence of -OOH and -OH groups in the oxidized products, as previously [28, 29, 32], we used the fast OH/OD exchange. To this end, 300 μL of D₂O (99.98%, Sigma-Aldrich) were introduced into 1 mL of oxidation samples (n-Hexane 2500 ppm, 600 K and 10 atm). We let reaction proceed for 20 min before analyses in FIA, UHPLC coupled with Orbitrap mass spectrometer using APCI (+/-) modes. A 2,4-DNPH derivatization was used in order to confirm the presence of carbonyl (ketone and aldehyde) function by formation of

DNPHydrazone derivatives (Fig. 1). The detailed mechanism is presented in Supplementary Material (Fig. S1). 20 μL of a diluted H_3PO_4 solution (50 μL of acid in 1 mL of ACN) and 100 μL of a saturated solution of 2,4-DNPH (2 g in 100 ml of ACN) were added to 1 ml of n-hexane oxidized sample (600K). Negative mode APCI was used to ionize DNPHydrazone derivatives.

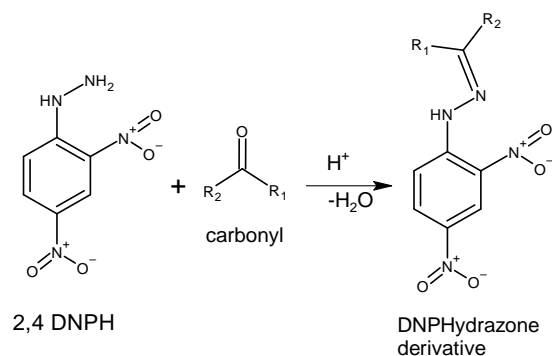


Fig. 1. Reaction of derivatization of carbonyl compounds with 2,4-DNPH.

3. Modeling

Simulations were conducted using PSR [46] from the Chemkin II package [47]. Third O_2 addition reactions were presented in the recent kinetic reaction mechanism proposed by Wang and Sarathy [14]. Low- and high-temperature chemistry are implemented in that scheme which involves 1188 species for 4959 reactions in total. The simulations showed that in the low-temperature oxidation region, n-hexane mainly reacts via H-atom abstraction by hydroxyl radicals coming from the decomposition of the $\text{KHP}^{2,4}$ and $\text{KHP}^{3,5}$ (Table 4). A shift in temperature was observed of all concentration profiles between the modeling and the experiments. The model predicts n-hexane oxidation starts $\sim 40\text{K}$ lower than in the experiments. In order to verify the validity of the present data, we repeated the experiments used to validate that model and found good agreement (Fig. 2) between three sets of experimental data obtained over a period of 6 years and using different JSR.

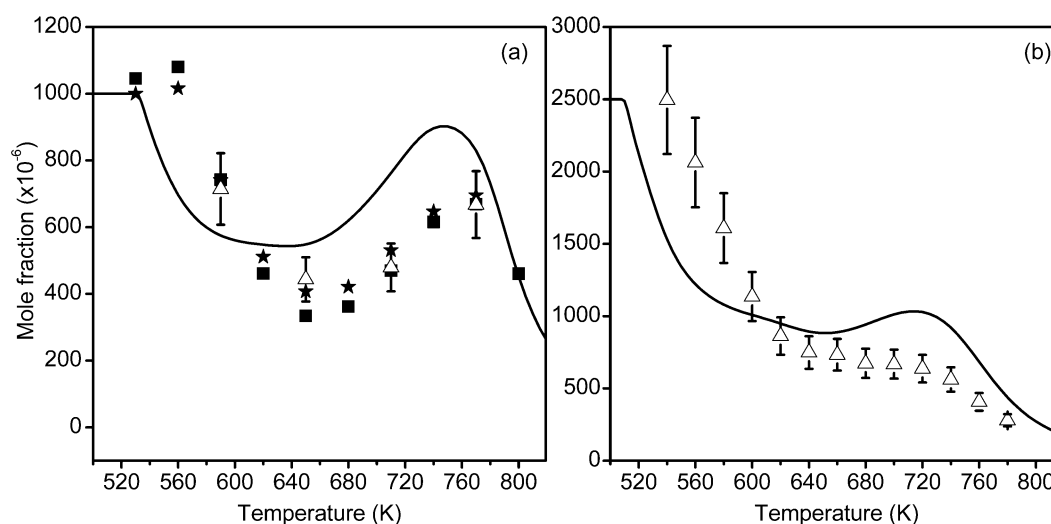


Fig. 2. Fuel profile for the oxidation of (a) 1000 ppm initial of n-hexane at a pressure of 10 atm, ($\phi = 0.5$, residence time of 0.7 s); other species profiles are presented in Figure S2 (Supplementary Material). (b) 2500 ppm of n-hexane ($\phi = 0.5$, residence time of 1.5 s). Open triangles are the present experiments, squares are the data from Zhang et al. [12], stars are unpublished data from our laboratory and the lines represent the modeling results using the mechanism proposed in [14].

Table 4. Structure of fuel's radicals, hydroperoxides and KHPs obtained by oxidation of n-hexane.

Initial radicals formed by H-atom abstraction on n-hexane		
Hydroperoxides deriving from the oxidation of n-hexyl radicals		
$\text{HOO-CH}_2\text{-CH}_2\text{-CH}_2\text{-CH}_2\text{-CH}_2\text{-CH}_3$	$\text{CH}_3\text{-CH(OOH)-CH}_2\text{-CH}_2\text{-CH}_2\text{-CH}_3$	$\text{CH}_3\text{-CH}_2\text{-CH(OOH)-CH}_2\text{-CH}_2\text{-CH}_3$
KHPs deriving from n-hexyl radicals' oxidation		

For temperature under ~ 900 K, the three hexyl radicals get peroxidized by reaction with O_2 . Three alkyl hydroperoxides can be produced after H-atom abstraction (Table 4). Internal H-shift in alkylperoxy radicals yields an alkyl hydroperoxyl radical. After a second addition of molecular oxygen followed by internal H-shift and decomposition, up to 15 keto-hydroperoxides can be produced (Table 4). The literature model considered here [14] includes the 3rd O_2 addition pathway yielding highly oxygenated products.

4. Results and discussion

n-Hexane oxidation was conducted in a JSR at 10 atm (Table 1). It yielded a wide range of products. Figure 3 presents a comparison of the present data obtained for the oxidation of 2500 ppm of n-hexane (see Table 1) and simulations. We can notice that the kinetic modeling fails to represent the production of some chemical species. For example, an overestimation of the formation of formic acid and an underestimation of acetic acid, methanol, and ethanol is noticeable. Underpredictions could be due to the absence of some reaction pathways in the kinetic model. The over-prediction of HCOOH , which at 600 K, is mainly produced via the oxidation of formaldehyde by OH^\bullet yielding $\text{HOCH}_2\text{O}^\bullet$, which in turn produces 72% of formic acid by decomposition, could be due to the use of inappropriate kinetics in the model. In the kinetic model, acetic acid formation proceeds through the decomposition of 4-hydroperoxyhexan-2-one (65%) and 3-hydroperoxyhexanal (35%). Possibly, additional pathways are required to increase acetic acid formation, or the rate constants used in the kinetic mechanism are too slow. In the kinetic model, at 600 K, methanol is mainly formed via three channels: self-reaction of $\text{CH}_3\text{OO}^\bullet$ (34%), H-atom abstraction by $\text{CH}_3\text{O}^\bullet$ on formaldehyde (32%), and reaction of $\text{CH}_3\text{OO}^\bullet$ with OH^\bullet (20%). At 600 K, the formation of ethanol is mainly due to H-atom abstraction by ethoxy radicals on methylhydroperoxy radicals (66%) and hydrogen peroxide (24%). The inclusion of other reactions of this type could increase ethanol production.

Figures 2 and 3 show that the kinetic model overestimates n-hexane oxidation rate below 620K. HRMS analyses allowed to observe many oxygenated products: $C_6H_{12}O_x$ ($x=1-7$), $C_6H_{10}O_x$ ($x=1-6$), $C_6H_8O_x$ ($x=1-6$), $C_6H_6O_x$ ($x=1-6$), $C_6H_4O_x$ ($x=3-5$), C_nH_{2n} ($n=4-6$), C_nH_{2n-2} ($n=4-6$), $C_nH_{2n}O$ ($n=3-6$), $C_nH_{2n-2}O$ ($n=3-6$), $C_nH_{2n-4}O$ ($n=3-6$), $C_nH_{2n+2}O_2$ ($n=6$), $C_nH_{2n}O_2$ ($n=2-6$), $C_nH_{2n-2}O_2$ ($n=3-6$), $C_nH_{2n-4}O_2$ ($n=3-6$), and $C_nH_{2n}O_3$ ($n=1-6$).

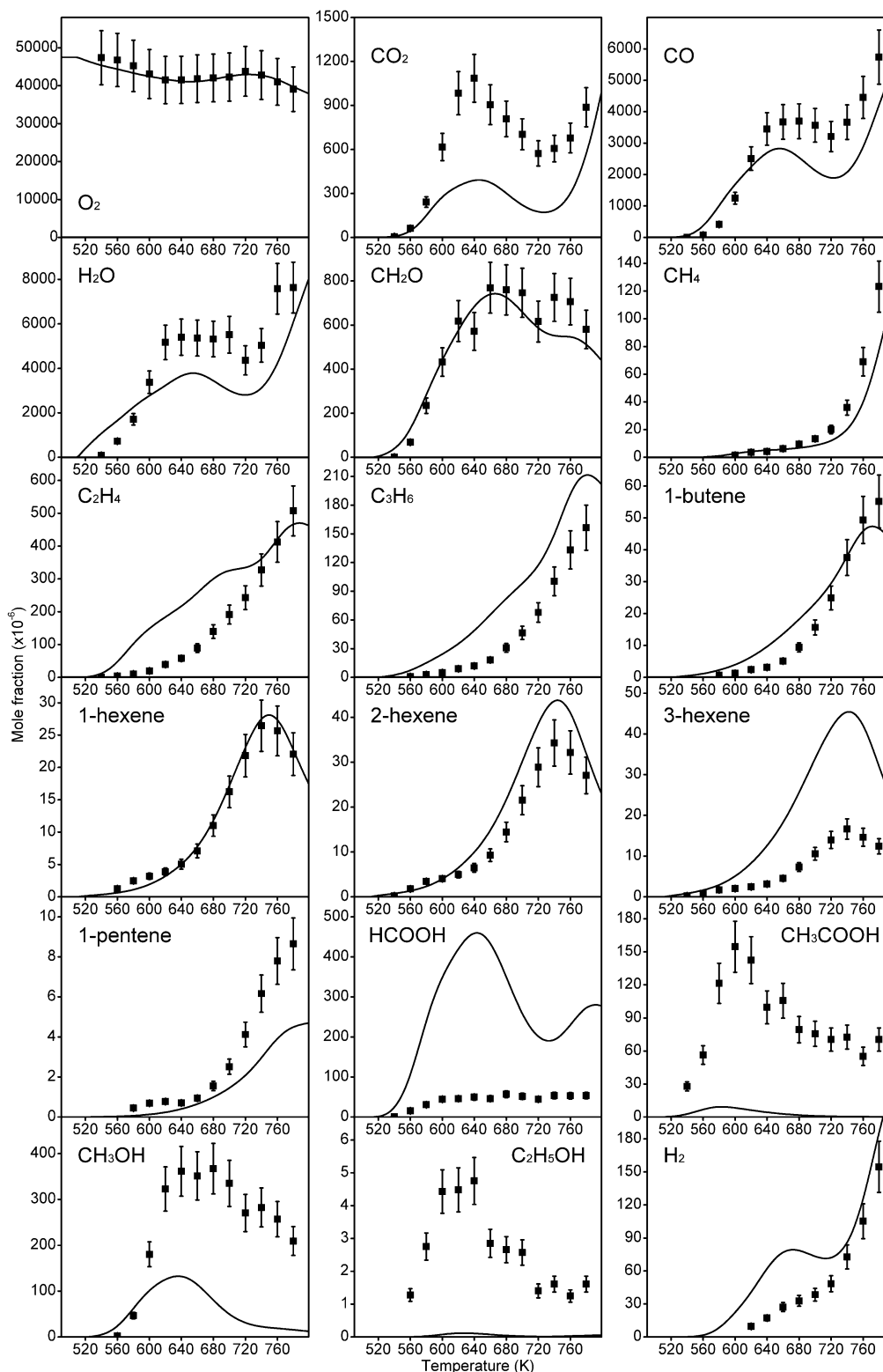
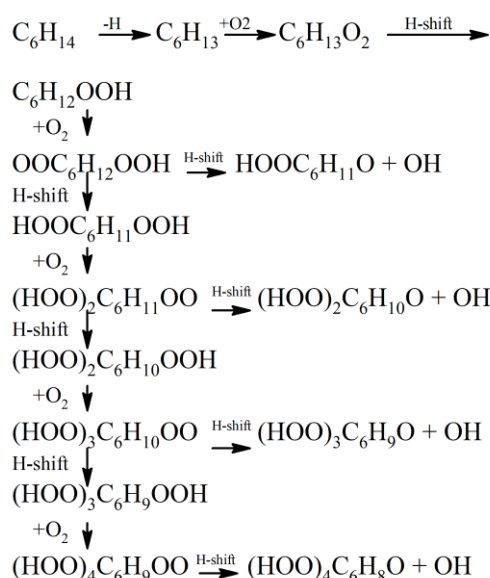


Fig. 3. Oxidation of 2500 ppm of n-hexane in a JSR (10 atm, $\phi = 0.5$, residence time of 1.5 s). Data obtained by GC-FID-TCD and FTIR (symbols) are compared to simulations using the model proposed earlier [14]. Results for the fuel are presented in Fig. 2b.

The present study indicated that besides keto-hydroperoxides, more oxygenated products are formed via multiple additions of O_2 on the fuel's radicals (R) and H-shifts (Scheme 1).



Scheme 1. Autoxidation pathways to ketohydroperoxides and HOMs after 4 molecular oxygen additions and multiple H-shifts.

In this study, we observed the products of second to 4th O_2 addition on the radicals from the fuel. The results presented in the next paragraphs confirm the extended oxidation pathways proposed earlier to rationalize experimental observations made in a JSR with molecular beam-time-of flight mass spectrometry-synchrotron vacuum ultraviolet photoionization [15, 28] and JSR-Orbitrap experiments [29, 32-34]. After the formation of peroxy radicals (RO_2), other oxygenated species are produced, such as alkyl-hydroperoxides: $\text{RO}_2 + \text{R}'\text{H} \rightarrow \text{ROOH} + \text{R}'$, $\text{RO}_2 + \text{HO}_2 \rightarrow \text{ROOH} + \text{O}_2$.

ROOH formation was detected here (Tables 4 and 5). Diols have the same global formula. It has been proposed that diols originate from di-hydroperoxides reactions [21].

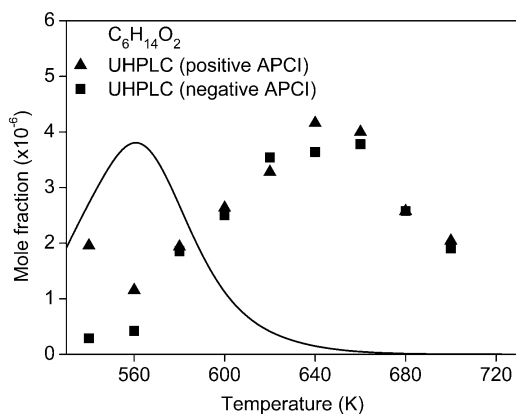


Fig. 4. Comparison of data (symbols: circle positive APCI, triangle negative APCI) and simulations (line) using the model of Wang [14]. The raw data are scaled to simulations using a mechanism proposed earlier [14]. Experimental errors are estimated to be less than 40%, as before [29, 32].

Their presence in the products could be verified by observing the formation of products of two H/D exchanges (Table 5). UHPLC/MS analyses using APCI (+/-) modes showed the presence of several chromatographic peaks with very low intensity, of the order of 10^4 (Supplementary Material, Fig. S3). This can be explained by the instability of hydroperoxides. Figure 4 shows the variation as a function of temperature of the integrated ROOH signal obtained by UHPLC-Orbitrap. Computations using a literature model [14] show a maximum difference of ~ 100 K between experimental and computed peak of concentration for ROOH. Rodriguez reported that the discrepancies between modeling and data could be reduced by increasing the activation energy of ROOH decomposition by several kcal/mol [48]. More temperature deviations between data and simulations were observed for other products, as presented in the next paragraphs.

ROOH can undergo H-atom abstraction followed by O_2 addition and intramolecular rearrangement reactions and form unsaturated ROOH or hexenyl hydroperoxides by two different mechanisms (Fig. 5). A signal

corresponding to $C_6H_{12}O_2$ species was detected in both positive ($C_6H_{13}O_2^+$, m/z 117.0910) and negative ($C_6H_{11}O_2^-$, m/z 115.0764) ionization modes. $C_6H_{12}O_2$ can also correspond to other molecules, such as hydroxy ketone/aldehyde. Unsaturated ROOH being less stable than hydroxy ketone/aldehyde molecules, comparison of $C_6H_{13}O_2^+$ chromatograms (Fig. 6) after a period of 7 weeks showed that some chromatographic peaks had decreased in intensity. Thus, the latter may correspond to unsaturated hydroperoxides (Rt 3 to 5 min). Stable compounds can correspond to hydroxy ketone/aldehydes. Furthermore, the DNPH derivatization allowed to observe the formation of many $C_6H_{12}O_2$ dinitrophenyl-hydrazone derivatives (which means the presence of a carbonyl function) (Supplementary Material, Fig. S4). The comparison between the different chromatographic peaks of $C_6H_{12}O_2$ (positive APCI $C_6H_{13}O_2^+$) before derivatization with DNPH and those remaining after derivatization, shows that the peaks which have not diminished (Rt 3 to 5 min), represent compounds which do not react with DNPH, the latter may be unsaturated hydroperoxides. However, the peaks whose intensity has decreased (Rt after 5 min) correspond to molecules having a ketone or aldehyde function which reacts with DNPH (Supplementary Material, Fig. S5).

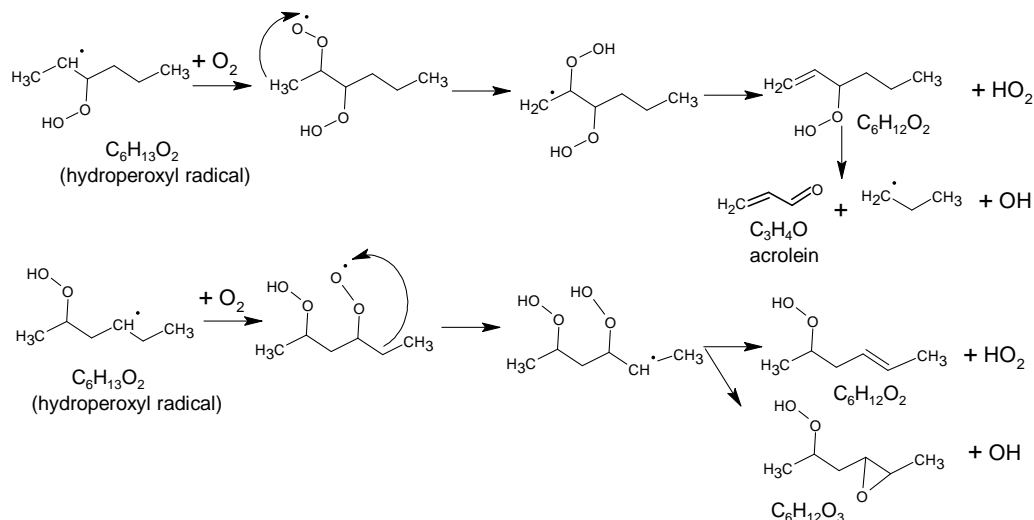


Fig. 5. Formation pathways for hexenyl hydroperoxides during the low temperature oxidation of n-hexane.

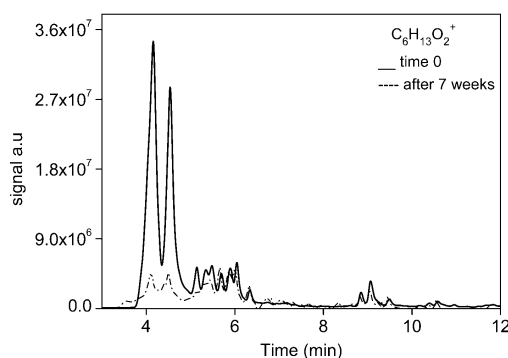


Fig. 6. Chromatograms showing formation of $C_6H_{12}O_2$. The analyses were performed using a C_{18} UHPLC-APCI (+) ($C_6H_{13}O_2^+$, m/z 117.0910). Comparison between analyses carried out shortly after sample collection and after 7 weeks.

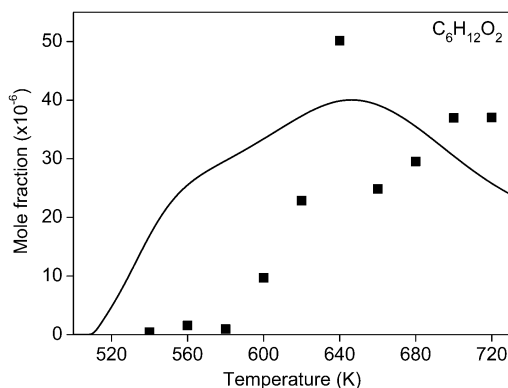


Fig. 7. Comparison of data (Orbitrap data scaled to modeling results, symbols) and modeling (line) of $C_6H_{12}O_2$ formed during oxidation of 2500 ppm of n-hexane ($\varphi = 0.5$, residence time of 1.5 s, and 10 atm).

Figure 7 shows reasonable agreement between modelling and experimental results, although the production of $C_6H_{12}O_2$ is overestimated below ca. 640 K. Table 5 summarizes the results obtained for the oxidation of 2500 ppm of n-hexane (See Table 1). The analyses were performed by FIA-HPCI +/-.

Table 5. Products of oxidation of 2500 ppm of n-hexane in a JSR at 600 K and 10 atm. H/D exchange done by addition of D_2O .

M (g/mole)	Compounds		Ionization mode			
			APCI (+)		APCI (-)	
	Formula	Name	m/z [M+H] ⁺	Signal (a.u)	m/z [M-H] ⁻	Signal (a.u)
56	C_3H_4O	Acrolein and isomers	57.0335	1.4E7	55.0232	1.5E4
60	$C_2H_4O_2$	Acetic acid and isomers	61.0283	3.1E5	59.0139	1.1E8
61	$C_2H_3D_1O_2$	Acetic acid-d ₁	62.0346	1.6E5	60.0201	7.2E8
74	$C_3H_6O_2$	Propanoic acid and isomers	75.0439	4.0E5	73.0295	5.7E7
75	$C_3H_5D_1O_2$	Propanoic acid and isomers-d ₁	76.0501	4.2E5	74.0358	3.7E6
88	$C_4H_8O_2$	Butyric acid and isomers	89.0594	4.1E5	87.0452	1.3E7
96	C_6H_8O	Keto hexadiene and hydroxy hexatriene	97.0646	3.5E7	95.0503	7.0E5
97	$C_6H_7D_1O$	hydroxy hexatriene-d ₁	98.0709	7.4E6	-	-
98	$C_6H_{10}O$	Keto hexene and hydroxy hexadiene	99.0802	3.2E8	97.0660	3.1E5
99	$C_6H_9D_1O$	hydroxy hexadiene-d ₁	100.0864	1.2E8	-	-
100	$C_6H_{12}O$	Cyclic ethers, hexanone and hexanal	101.0958	6.7E7	99.0816	5.3E3
101	$C_6H_{11}D_1O$	Hexanal-d ₁	102.1020	3.8E7	100.0877	2.6E3
114	$C_6H_{10}O_2$	Hexanedione and keto-enols	115.0753	4.6E8	113.0609	7.7E7
115	$C_6H_9D_1O_2$	Keto-enols-d ₁	116.0812	5.5E8	114.0671	1.7E7
116	$C_6H_{12}O_2$	Unsaturated ROOH, Hydroxy ketone/aldehyde and hexanoic acid	117.0908	2.6E7	115.0765	9.7E5
117	$C_6H_{11}D_1O_2$	Hexanoic acid and isomers-d ₁	118.0968	4.6E6	116.0828	3.0E4
118	$C_6H_{14}O_2$	Diol-ROOH	119.1063	4.6E4	117.0923	2.8E3
119	$C_6H_{13}D_1O_2$	Diol-ROOH-d ₁	120.1126	1.0E4	-	§
120	$C_6H_{12}D_2O_2$	Diol-d ₂	121.1188	8.0E2	-	§
128	$C_6H_8O_3$	Triketones and diketo-enols	129.0543	1.2E7	127.0401	3.4E8
129	$C_6H_7D_1O_3$	diketo-enols-d ₁	130.0606	9.5E6	128.0464	1.7E8
130	$C_6H_{10}O_3$	Unsaturated KHP and keto-acid	131.0701	8.2E6	129.0557	1.9E8
131	$C_6H_9D_1O_3$	Unsaturated KHP and Keto acid-d ₁	132.0762	1.1E7	130.0619	9.6E7
132	$C_6H_{12}O_3$	Keto-hydroperoxide	133.0856	1.3E6	131.0713	9.7E7
133	$C_6H_{11}D_1O_3$	Keto-hydroperoxide-d ₁	134.0918	2.5E6	132.0777	4.7E7
142	$C_6H_6O_4$	Tetraketone	143.0336	5.6E4	141.0193	2.9E7
146	$C_6H_{10}O_4$	Diketo-hydroperoxide	147.0648	2.3E6	145.0506	8.8E7
147	$C_6H_9D_1O_4$	Diketo-hydroperoxide-d ₁	148.0711	4.1E6	146.0569	2.6E7
148	$C_6H_{12}O_4$	Hydroxy ketohydroperoxides	149.0805	2.6E4	147.0662	2.3E6
149	$C_6H_{11}D_1O_4$	Hydroxy ketohydroperoxides-d ₁	150.0868	1.1E5	148.0725	2.0E6
150	$C_6H_{10}D_2O_4$	Hydroxy ketohydroperoxides-d ₂	151.0931	7.2E4	149.0788	3.5E5
160	$C_6H_8O_5$	Tri keto-hydroperoxide	161.0442	3.3E3	159.0299	1.2E7
161	$C_6H_7D_1O_5$	Tri keto-hydroperoxide-d ₁	-	§	160.0362	1.4E6
164	$C_6H_{12}O_5$	Keto-dihydroperoxides	165.0767	3.9E3	163.0612	1.2E6
165	$C_6H_{11}D_1O_5$	Keto-dihydroperoxides-d ₁	-	§	164.0675	3.3E5
166	$C_6H_{10}D_2O_5$	Keto-dihydroperoxides-d ₂	-	-	165.0740	3.2E3
178	$C_6H_{10}O_6$	Diketo-dihydroperoxides	-	-	177.0405	4.7E5
179	$C_6H_9D_1O_6$	Diketo-dihydroperoxides-d ₁	-	-	178.0468	1.8E5
180	$C_6H_8D_2O_6$	Diketo-dihydroperoxides-d ₂	-	-	179.0531	1.6E4
180	$C_6H_{12}O_6$	Hydroxy keto dihydroperoxides	-	-	179.0561	3.1E5
181	$C_6H_{11}D_1O_6$	Hydroxy keto dihydroperoxides-d ₁	-	-	180.0624	3.8E5

182	C ₆ H ₁₀ D ₂ O ₆	Hydroxy keto dihydroperoxides-d ₂	-	-	181.0687	7.6E4
183	C ₆ H ₉ D ₃ O ₆	Hydroxy keto dihydroperoxides-d ₃	-	-	182.0752	5.4E3
196	C ₆ H ₁₂ O ₇	Keto-trihydroperoxides	-	-	195.0511	4.9E4
197	C ₆ H ₁₁ D ₁ O ₇	Keto-trihydroperoxides-d ₁	-	-	196.0573	7.9E4
198	C ₆ H ₁₀ D ₂ O ₇	Keto-trihydroperoxides-d ₂	-	-	197.0636	1.5E4
199	C ₆ H ₉ D ₃ O ₇	Keto-trihydroperoxides-d ₃	-	-	198.0698	§
210	C ₆ H ₁₂ O ₈	Hydroxy keto trihydroperoxides	-	-	211.0459	5.2E3
211	C ₆ H ₁₁ D ₁ O ₈	Hydroxy keto trihydroperoxides-d ₁	-	-	212.0525	1.1E4
212	C ₆ H ₁₀ D ₂ O ₈	Hydroxy keto trihydroperoxides-d ₂	-	-	213.0584	§
213	C ₆ H ₉ D ₃ O ₈	Hydroxy keto trihydroperoxides-d ₃	-	-	214.0647	§

Note: § under limit of detection; - Not detected.

C₁₈-UHPLC-MS-APCI (+) analyses of C₆H₁₂O₃ (C₆H₁₃O₃⁺, *m/z* 133.0856) showed the presence of several chromatographic peaks that could be KHPs or other chemical species having the same exact mass (Fig. 8a). Gaussian curve fitting algorithm was applied to separate the different contributions of the isomers in order to calculate peaks areas and plotting their different profiles as a function of temperature. Thus, the peaks having the same trend as the KHPs modeling were attributed to KHPs (Fig. 8a, peaks # 1, 2, 5, 6, 7, 8, and 9). The data were compared to the KHPs modeling profile (Fig. 8b). C₆H₁₃O₃⁺ (*m/z* 133.0856) MS/MS analyses (HCD 10 eV) produced several fragments, some were identified and confirm the molecular structure of KHPs (Table 6). Some fragments may be common to several KHP isomers. For example: C₆H₁₁O₂⁺ (*m/z* 115.0749), C₃H₇O⁺ (*m/z* 59.0490), C₃H₅O⁺ (*m/z* 57.0334), and C₂H₅O₂⁺ (*m/z* 61.0283). However, some fragments (C₄H₉O, *m/z* 73.0645 and C₄H₇O₂, *m/z* 87.0438) could not be used for the identification of KHPs isomers; these could result from intramolecular rearrangements.

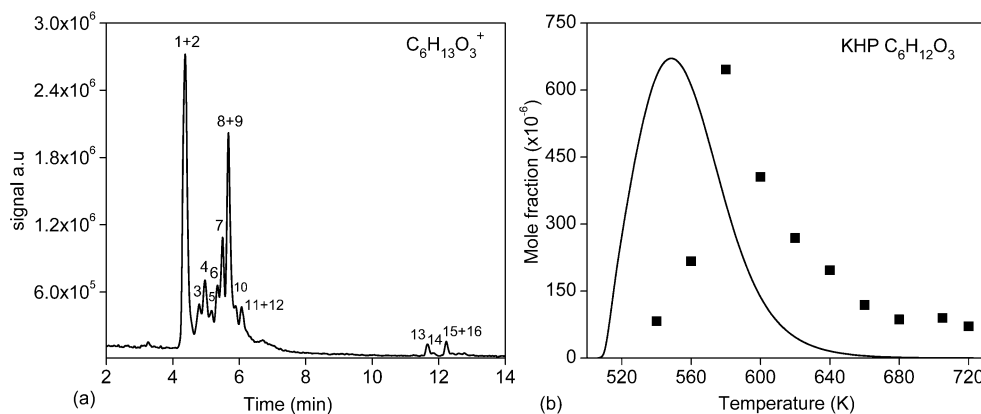


Fig. 8. (a) Chromatographic separation C₆H₁₂O₃ (C₆H₁₃O₃⁺ *m/z* 133.0856) isomers obtained by n-hexane oxidation at 600 K. C₁₈ UHPLC-APCI positive mode was used. (b) Formation of C₆H₁₂O₃ KHPs: comparison of UHPLC data (scaled to modeling results, symbols) and modeling (line) using the model of Wang [14]. The data were obtained by integration of UHPLC-HRMS APCI (+) signal (*m/z* 133.0859) and scaled to the computed maximum concentration. Experimental errors are estimated to be less than 40%, as earlier [29, 32].

The signal attributed to KHPs abruptly increases below the ceiling temperature. It reaches a maximum at a temperature corresponding to ~60% conversion of n-hexane (~590 K). Such matching has been observed earlier in JSR experiments conducted near 1 bar (~550 K [49] and ~530 K [15]). Figure 8b shows a comparison of the experimental results (positive mode APCI) for the sum of the 7 KHPs and the simulations for n-heptane determined under JSR conditions. This figure shows that the reaction mechanism used here [14] predicts the variation of KHPs concentration as a function of temperature in the cool flame regime, while the computed mole fraction profile is shifted towards lower temperatures in comparison with the data.

Table 6. Structure of observed fragments in MS/MS analyses (HCD 10eV) of C₆H₁₂O₃ KHP isomers in APCI positive mode (C₆H₁₃O₃⁺, *m/z* 133.0856).

<i>m/z</i> and molecular formula	molecular structures
57.0334 C ₃ H ₅ O	
61.0283 C ₂ H ₅ O ₂	
99.0804 C ₆ H ₁₁ O Loss of OOH	
115.0749 C ₆ H ₁₁ O ₂ Loss of H ₂ O and intramolecular rearrangement	
59.0490 C ₃ H ₇ O	

The Korcek mechanism [50] transforms γ -keto-hydroperoxides into a range of more stable products (ketones/aldehydes and acids). This pathway can modify the global rate of fuel ignition [14]. Computations on C₃ γ -KHPs unimolecular reactions [51] have demonstrated that among 75 possible reactions, the Korcek mechanism had the lowest transition state energy. Several ketones and carboxylic acids can derive from n-hexane's γ -KHP decomposition, e.g., 2-butanone and acetic acid, acetone and propanoic acid, acetaldehyde and butyric acid (Fig. 9).

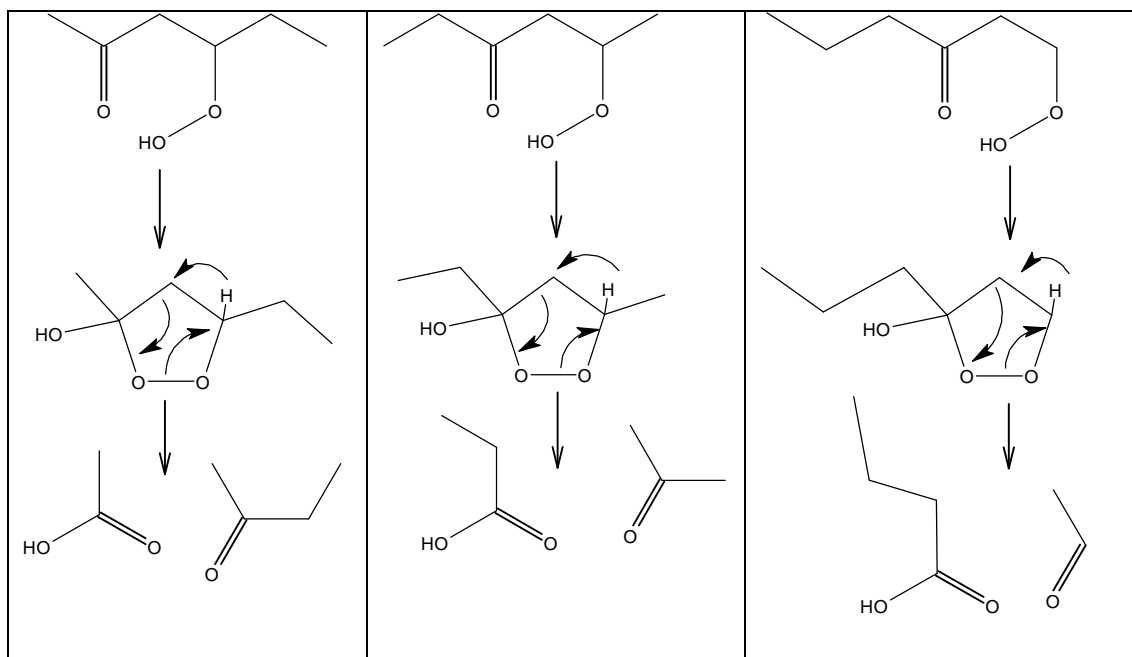


Fig. 9. The Korcek mechanism for most probable n-hexane's γ -keto-hydroperoxides.

In Fig. 10 we present the formation of ketones/aldehydes and carboxylic acids detected as a function of temperature.

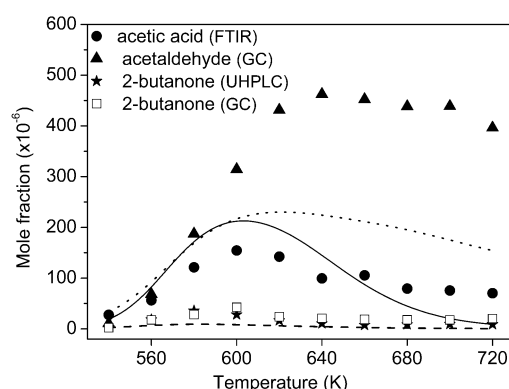
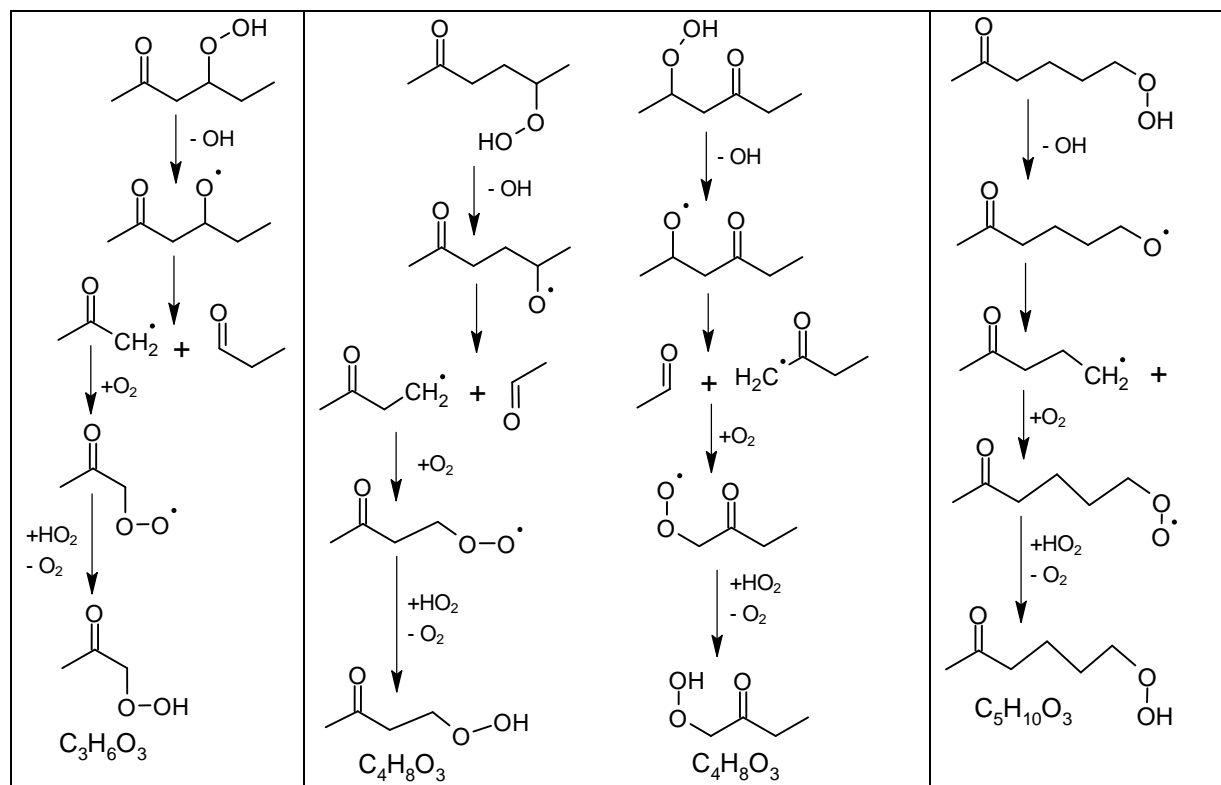


Fig. 10. Acids and ketones potentially produced through the Korcek mechanism during the oxidation of 2500 ppm of n-hexane in a JSR (see Table 1). Data obtained by GC, FTIR and UHPLC (symbols) are compared to modeling results (continuous line: 2-butanone, dotted lined: acetaldehyde, and dashed line: acetic acid). UHPLC-MS analyses were conducted in APCI positive mode and the data were scaled to the corresponding quantitative GC and FTIR data.

Figure 10 presents the concentration profiles for the acid-ketones/aldehyde pairs which could be formed through the Korcek mechanism ($C_2H_4O_2/C_4H_8O$, $C_3H_6O_2/C_3H_6O$, and $C_4H_8O_2/C_2H_4O$). The different analyses (UHPLC Orbitrap, FTIR and GC-MS) did not allow the detection of butyric acid. Propanoic acid and acetone signals were detected in UHPLC Orbitrap (+/-) modes. However, their profiles could not be plotted due to co-elution (co-elution of acetone and propionaldehyde). Nevertheless, we could observe that the intensity of DNPH-acetone is way less intense than that of DNPH-propionaldehyde (Supplementary Material, Table S2). Therefore, if the formation of acetone occurs via the Korcek route, it should be of minor importance here. The decomposition of the most favorable KHP via the Korcek mechanism, KHP^{2,4}, would yield acetic acid and 2-butanone. These products were observed, with predominance of the acid. If the small production of 2-butanone is attributed to the Korcek mechanism, again, it seems it is of minor importance whereas acetic acid can be produced through other routes. The comparison between modeling and experimental profiles of the species which could be formed through the Korcek mechanism reveals an overestimation of the production of 2-butanone by the kinetic model. Conversely, acetaldehyde and acetic acid concentrations are underpredicted by the model.

KHPs ($C_6H_{12}O_3$) may react via other reaction pathways. They can form lower mass KHPs ($C_3H_6O_3$, $C_4H_8O_3$ and $C_5H_{10}O_3$) according to the mechanism proposed earlier [14] (Table 7).

Table 7. Formation of $C_3H_6O_3$, $C_4H_8O_3$ and $C_5H_{10}O_3$ KHP's isomers formed by decomposition of $C_6H_{12}O_3$ KHPs during the oxidation of n-hexane:



According to the kinetic scheme proposed earlier [14] the formation of three $C_3H_6O_3$, five $C_4H_8O_3$, and ten $C_5H_{10}O_3$ KHPs occurs in the following order of importance $C_3H_6O_3 \gg C_4H_8O_3 > C_5H_{10}O_3$. UHPLC-MS APCI (+) analyses revealed chromatographic peaks corresponding to these different KHPs, two peaks for $C_3H_6O_3$ ($C_3H_7O_3^+$, m/z 91.0388), three peaks for $C_4H_8O_3$ ($C_4H_9O_3^+$, m/z 105.0545) and five peaks for $C_5H_{10}O_3$ ($C_5H_{11}O_3^+$, m/z 119.0702). The presence of a ketone function in these products was confirmed by DNPH derivatization (Supplementary Material Table S1). UHPLC-HRMS analyses showed that the concentrations of C_3 , C_4 , and C_5 KHPs reach a maximum at 600 K (Fig. 11).

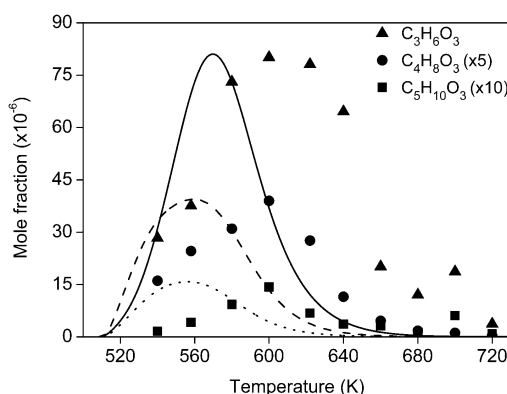


Fig.11. Concentration profiles for C_3 , C_4 , and C_5 KHPs ($C_3H_7O_3^+$, m/z 91.0388), $C_4H_8O_3$ ($C_4H_9O_3^+$, m/z 105.0545) and $C_5H_{10}O_3$ ($C_5H_{11}O_3^+$, m/z 119.0702). Comparison between UHPLC Orbitrap experimental data scaled to modeling results (symbols) and modeling ($C_3H_6O_3$: continuous line, $C_4H_8O_3$: dashed line, and $C_5H_{10}O_3$: dotted line), respectively.

n-Hexane oxidation at low temperature leads to the formation of other chemical species. Indeed, several aldehydes (formaldehyde, acetaldehyde, acrolein, propionaldehyde, crotonaldehyde, etc.), ketones (2-pentanone, 2-hexanone and 3-hexanone, Methyl vinyl ketone noted MVK) and diones (2,4-pentanedione) were identified by comparison to pure standards or by DNPH derivatization and comparison with DNPHhydrazone standards (either if carbonyl

standard is not available or carbonyl mass is <50 uma). Tables S2 and S3 (Supplementary Material) illustrate the identification of the different carbonyl compounds. Examples of comparison of MVK, methyloxirane, 2-pentanone, and 2,4-pentanedione signals variation profiles obtained using UHPLC-HRMS and GC-MS are shown in Fig.12. As for several chemical species mentioned previously, we noticed that there is a difference (~80 K) between experimental and predicted peak concentration of MVK. The present model predicts the formation of MVK results from the oxidation of 2-butanone (97%) and 2,3-epoxyhexane (3%). Formation pathways are given in Scheme 2.

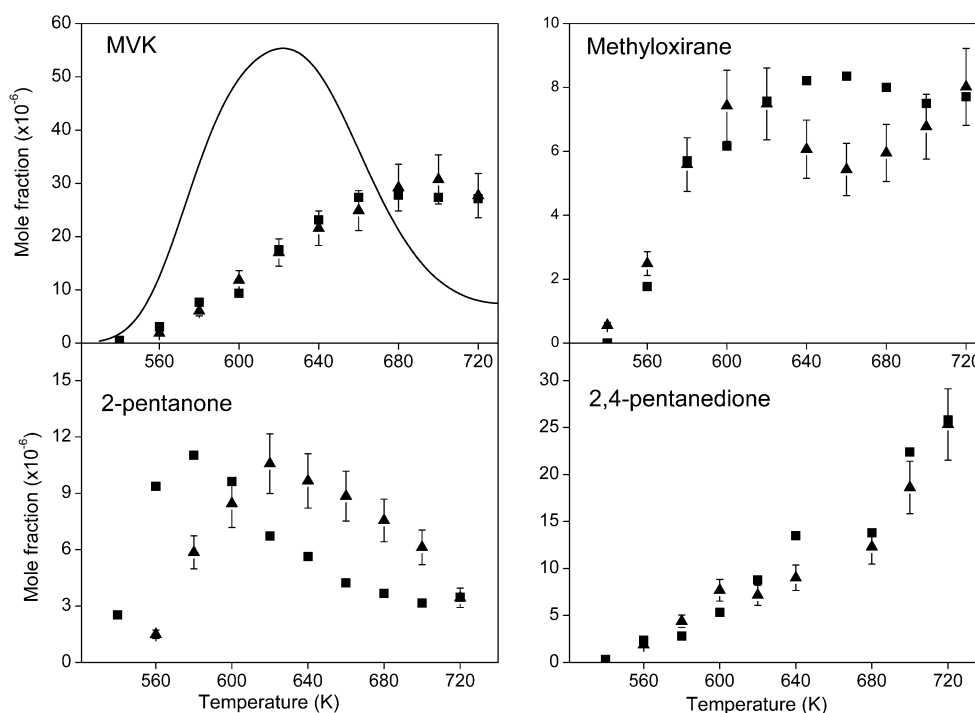
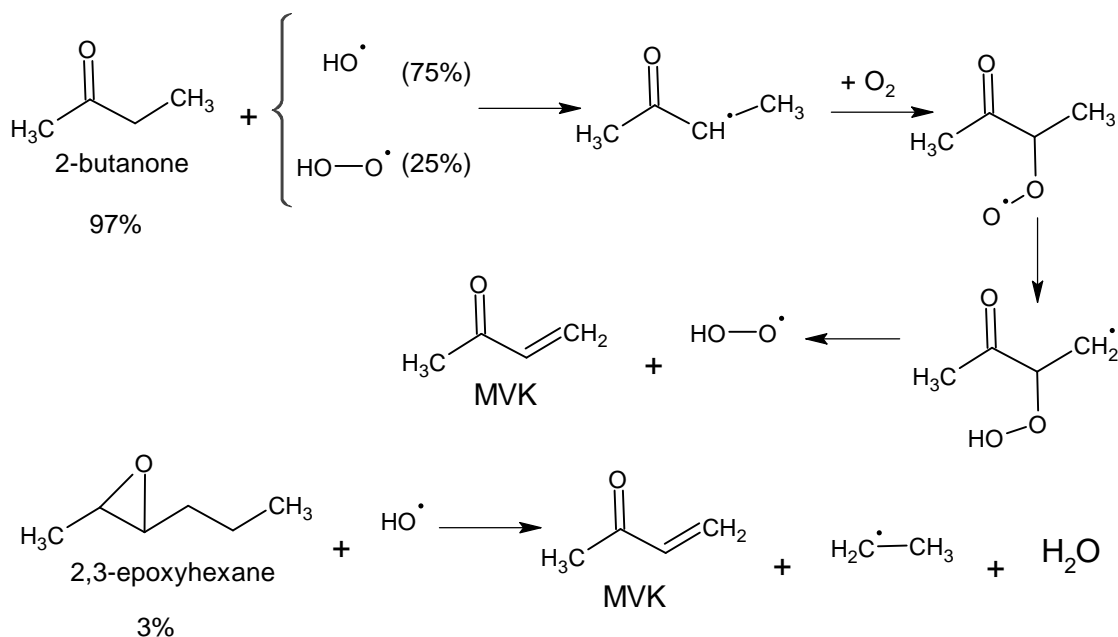


Fig.12. Formation of MVK ($C_4H_7O^+$, m/z 71.0491), methyloxirane ($C_3H_7O^+$, m/z 59.0491), 2-pentanone ($C_5H_{11}O^+$, m/z 87.0804) and 2,4-pentanedione ($C_5H_9O_2^+$, m/z 101.0596). Comparison between experimental data (UHPLC-HRMS-APCI+, squares and GC, triangles) and modeling results (line) for MVK.



Scheme 2. Formation pathways of MVK during low temperature oxidation of n-hexane.

It has been proposed that diones are produced through the decomposition of KHPs [52], or directly produced by H-atom abstraction on KHPs. [53]: $R\cdot + C_6H_{12}O_3^{ij} \rightarrow RH + C_6H_{10}O_2^{ij} + OH\cdot$

(i and j represent the positions of carbonyl and OOH groups in KHPs). Roaming reactions of KHPs [54] to produce a dione and water, and $\cdot\text{OOQOOH}$ decomposition [55] have also been proposed to explain diones formation.

Here, several diones were observed as a function of temperature using UHPLC-MS analyses (Fig. 13a). Figures 13b and 13c show the variation of 2,5-hexanedione (Rt 4.17 min) and 2,4-hexanedione (Rt 4.35 min) signal ($\text{C}_6\text{H}_{11}\text{O}_2^+$ m/z 115.0753). As noticed for several other cool flame products, experimentally, the formation of diones peaks around 580K. UHPLC-MS analyses using negative APCI (Fig. 13a) reveal the presence of other $\text{C}_6\text{H}_{10}\text{O}_2$ isomeric compounds which can be keto-enols. This possibility was verified by the occurrence of an H/D exchange (Table 5).

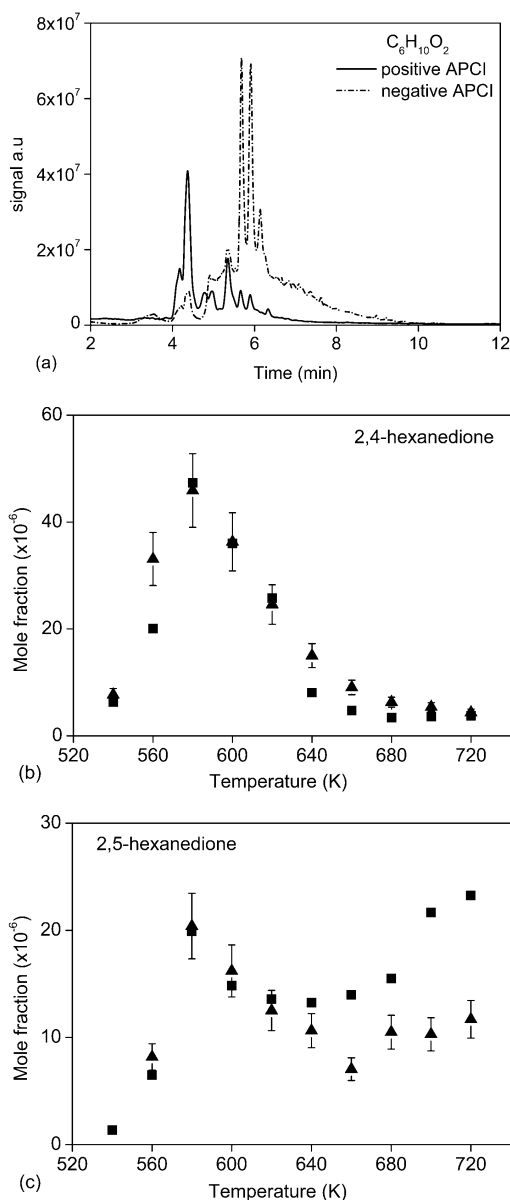


Fig. 13. Diones $\text{C}_6\text{H}_{10}\text{O}_2$ formation during n-hexane oxidation in a JSR: (a) chromatogram showing $\text{C}_6\text{H}_{10}\text{O}_2$ using C_{18} UHPLC-APCI analyses: full line APCI (+) m/z 115.0753, $\text{C}_6\text{H}_{11}\text{O}_2^+$, dotted line APCI (-) m/z 113.0609, $\text{C}_6\text{H}_9\text{O}_2^-$. (b) profile of 2,4-hexanedione, (c) profile of 2,5-hexanedione obtained by UHPLC-HRMS (square), GC-MS (triangle) analyses. HRMS data are scaled to the corresponding quantitative GC data.

During n-hexane oxidation, several cyclic ethers can be produced in the NTC region. They are formed by decomposition of alkyl hydroperoxides: $\text{QOOH} \rightarrow \text{cyclic ether} + \text{OH}$.

UHPLC-MS signal corresponding to $\text{C}_6\text{H}_{12}\text{O}$ isomers was detected in APCI +/- (m/z 101.0960, $\text{C}_6\text{H}_{13}\text{O}^+$) and (m/z 99.0816 $\text{C}_6\text{H}_{11}\text{O}^-$), see Fig. 14a. The cyclic ethers profiles obtained by UHPLC-MS analysis were compared to the modeling and to total signal of 2,5-dimethyl-THF and 2-butyloxirane obtained by GC-MS (Fig. 14b).

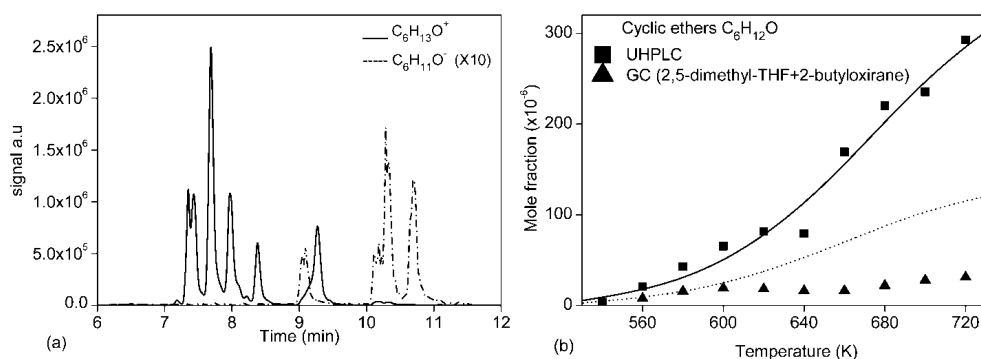


Fig. 14. Cyclic ethers' formation during n-hexane oxidation in a JSR. (a) Chromatograms for $C_6H_{12}O$ showing different isomers formed at 720 K: 2,5-dimethyl-THF trans & cis (Rt 7.67 and 7.97 min), 2-butyloxirane (10.13 min), 2-hexanone (9.02 min), 3-hexanone (9.26 min) and hexanal (10.64 min). Analyses were conducted in APCI (+/-) modes $C_6H_{13}O^+$, m/z 101.0960 and $C_6H_{11}O^+$, m/z 99.0816. (b) Comparison between experimental signal (symbols): UHPLC (data scaled to modeling results, cyclic ethers integrated signal) and GC (2,5-dimethyl-THF and 2-butyloxirane) compared to modeling results: total cyclic ethers (line), and sum of 2,5 dimethyl-THF and 2-butyloxirane (dash).

$C_6H_{12}O$ can also correspond to hexanone and hexanal. These molecules have been identified using standards. UHPLC-MS and GC-MS analyses allowed observing the variation of their concentrations during the cool-flame oxidation of n-hexane over the temperature range 540 to 720K (Fig. 15).

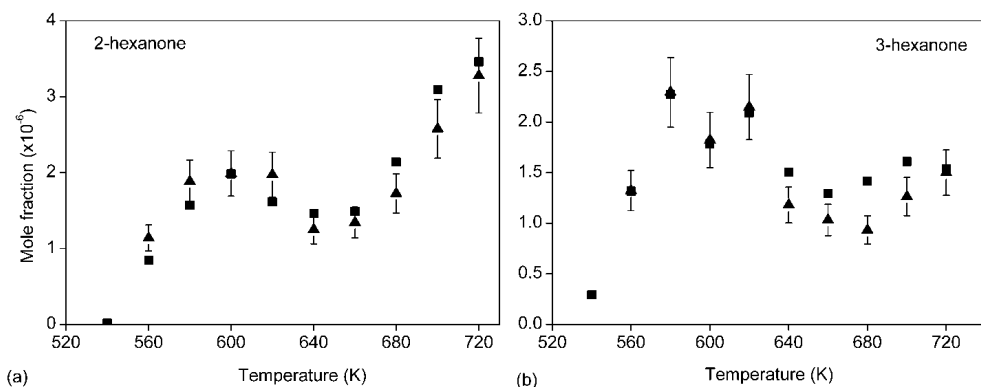


Fig. 15. Formation of (a) 2-hexanone and (b) 3-hexanone during the oxidation of 2500 ppm of n-hexane in a JSR. UHPLC APCI (+) mode (m/z 101.0960, $C_6H_{13}O^+$) (square symbols, scaled to quantitative GC data) compared to GC-MS analyses (triangle symbols).

Figure 15 shows that 2-hexanone and 3-hexanone have two formation phases, which implies two different chemical pathways over the low temperature oxidation of n-hexane. The first 2-hexanone formation peaks at a temperature around 600 K. The MS signal decreases between 620 and 640 K and then increases again between 640 and 720 K. The 3-hexanone MS signal behaves similarly.

Thanks to the use FIA and UHPLC APCI (+/-), different hexenones were detected. For instance, keto hexene $C_6H_{10}O$ ($C_6H_{11}O^+$ m/z 99.0802, $C_6H_9O^+$ m/z 97.0660) (Fig.16a and b) and keto hexadiene C_6H_8O ($C_6H_9O^+$, m/z 97.0646; $C_6H_7O^+$, m/z 95.0503), see Fig. 17a and b. The presence of a carbonyl group has been confirmed by DNPH derivatization (Supplementary Material, Table S1). However, the comparison of $C_6H_{10}O$ (Fig. 16b) and C_6H_8O (Fig.17b) chromatographic peaks before and after DNPH derivatization show a decrease of only some peaks corresponding to isomers with a carbonyl function ($C_6H_{10}O$ keto hexene and C_6H_8O keto hexadiene), which indicates that the other peaks (not reacting with DNPH) correspond to different $C_6H_{10}O$ and C_6H_8O isomers. For example, the presence of hydroxy hexadiene, $C_6H_{10}O$, and hydroxy hexatriene, C_6H_8O , could be responsible for the observed H/D exchange reported in Table 5.

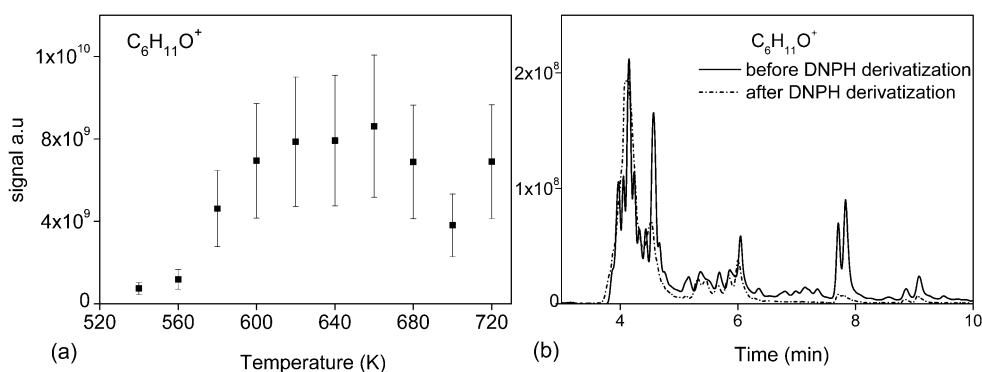


Fig. 16. Formation of $C_6H_{10}O$ during n-hexane oxidation. (a) Variation of keto hexene as a function of JSR temperature. (b) Chromatographic peaks showing variation of the $C_6H_{10}O$ signal ($C_6H_{11}O^+$, m/z 99.0802) before and after DNP derivatization. Keto hexenes correspond to peaks with decreasing intensity after DNP derivatization.

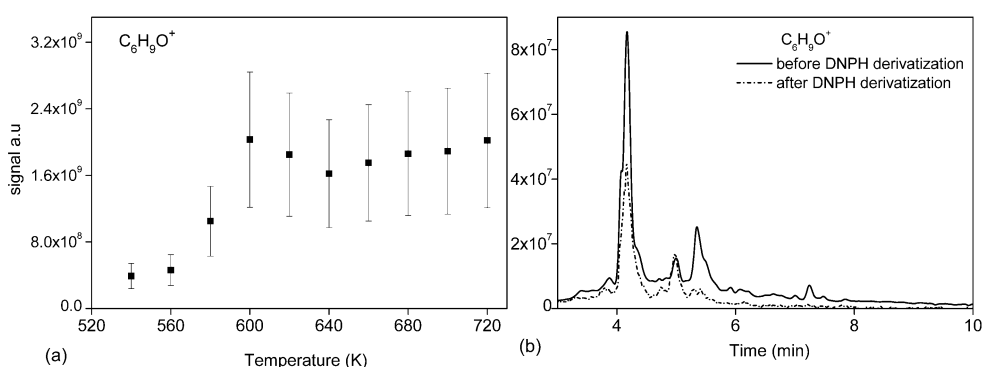
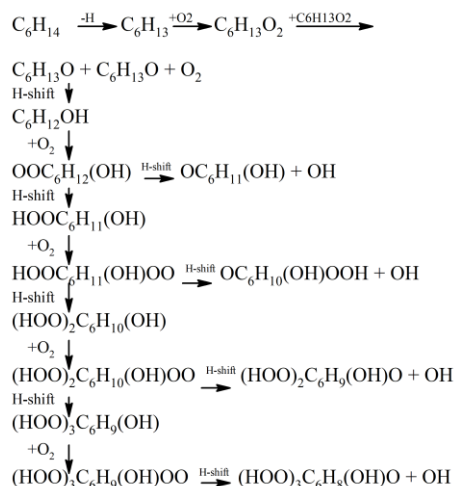


Fig. 17. Formation of C_6H_8O during n-hexane oxidation. (a) Variation of keto hexadiene as function as JSR temperature. (b) Chromatographic peaks showing variation of C_6H_8O concentrations ($C_6H_9O^+$ m/z 97.0646) before and after DNP derivatization. Keto hexadienes correspond to peaks with decreasing intensity after DNP derivatization.



Scheme 3. Peroxy radicals' oxidation pathways commonly considered in atmospheric chemistry, ultimately yielding HOMs.

Other oxidation pathways for peroxy radicals can occur. Scheme 3 presents one of them which proceeds via the formation of alkoxy radicals which react via sequential H-shifts and O_2 additions. The products of this reaction pathway consisting of $C_6H_{12}O_{2,4,6,8}$ were observed in the present experiments (Table 5). In addition to all the chemical species reported in this paper, other highly oxygenated molecules have been detected, such as $C_6H_{10}O_3$ (unsaturated KHPs and keto acids, MW 130), $C_6H_8O_3$ (triketone and diketo-enols, MW 128), $C_6H_8O_5$ (Triketo hydroperoxides, MW 160), as well as the other formula listed in Table 5.

5. Conclusion and Perspectives

n-Hexane oxidation was conducted in a JSR at 10 atm and an equivalence ratio of 0.5 (540-720 K, residence time of 1.5 s and initial fuel concentration of 2500 ppm; 530-800 K, residence time of 0.7 s and 1000 ppm of fuel). Cool-flame products formed in JSR experiments were characterized after collection of samples dissolved in cooled acetonitrile. These liquid samples were analyzed using several analytical techniques (FIA and UHPLC analyses coupled with high resolution mass spectrometry using APCI in both positive and negative modes). All of these analyses allowed characterizing hydroperoxides ($C_6H_{14}O_2$), unsaturated hydroperoxides ($C_6H_{12}O_2$), keto-hydroperoxides ($C_6H_{12}O_3$), ketohydroperoxides ($C_3H_6O_3$, $C_4H_8O_3$, $C_5H_{10}O_3$) resulting from decomposition of KHPs $C_6H_{12}O_3$, diones ($C_6H_{10}O_2$), Cyclic ethers and C_6 -ketones ($C_6H_{12}O$). Also, highly oxygenated molecules were detected ($C_6H_{12}O_{4-8}$). Carbonyl compounds were characterized by DNPH derivatization. To verify the presence of hydroxyl or hydroperoxyl groups in n-hexane oxidized products, H/D exchange with D_2O was used. MS-MS analyses were used to try to identify the KHPs isomers.

Additional experiments using complementary techniques are planned to better assess the reaction pathways of n-hexane oxidation in cool flames, e.g., JSR-MS-ToF-synchrotron photoionization, sampling in piston engines. Also, the characterization of HOMs using recently developed strategies [42] are currently applied to a range of fuels, including n-hexane. These studies are expected to further confirm similitudes in terms of products of oxidation formed in combustion and in the troposphere.

Acknowledgements

The authors gratefully acknowledge funding from the Labex Caprysses (convention ANR-11-LABX-0006-01) and from the Région Centre Val de Loire, EFRD, and CPER (projects PROMESTOCK and APROPOR-E).

References

- [1] P. Dagaut; M. Cathonnet, The ignition, oxidation, and combustion of kerosene: A review of experimental and kinetic modeling, *Prog. Energy Combust. Sci.* 32 (1) (2006) 48-92.
- [2] W. J. Pitz; C. J. Mueller, Recent progress in the development of diesel surrogate fuels, *Prog. Energy Combust. Sci.* 37 (3) (2011) 330-350.
- [3] P. Dagaut, On the kinetics of hydrocarbons oxidation from natural gas to kerosene and diesel fuel, *Phys. Chem. Chem. Phys.* 4 (11) (2002) 2079-2094.
- [4] C. Bayındırlı; M. Celik; M. Demiralp; İ. Ors, Investigation Of Effect Of n-Hexane Additives In Biodiesel On Combustion And Exhaust Emissions In Diesel Engines, *International Journal of Automotive Engineering and Technologies* 6 (3) (2017) 140-147.
- [5] M. Çelik; C. Bayindirli, Enhancement performance and exhaust emissions of rapeseed methyl ester by using n-hexadecane and n-hexane fuel additives, *Energy* 202 (2020) 117643.
- [6] C. Bayındırlı; M. Celik, Investigation of combustion and emission characteristics of n-hexane and n-hexadecane additives in diesel fuel, *Journal of Mechanical Science and Technology* 33 (4) (2019) 1937-1946.
- [7] A. Burcat; E. Olchanski; C. Sokolinski., *Isr. J. Chem.* 36 (1996) 313-320.
- [8] V.P. Zhukov; V. A. Sechenov; A. Y. Starikovskii, Ignition delay times in lean n-hexane-air mixture at high pressures, *Combust. Flame* 136 (2004) 257-259.
- [9] R. Mevel; K. Chatelain; P. A. Boettcher; G. Dayma; J. E. Shepherd, Low temperature oxidation of n-hexane in a flow reactor, *Fuel* 126 (2014) 282-293.
- [10] Z. Wang; O. Herbinet; Z. Cheng; B. Husson; R. Fournet; F. Qi; F. Battin-Leclerc, Experimental Investigation of the Low Temperature Oxidation of the Five Isomers of Hexane, *J. Phys. Chem. A* 118 (2014) 5573-5594.
- [11] F. Qi, Combustion chemistry probed by synchrotron VUV photoionization mass spectrometry, *Proc. Combust. Inst.* 34 (2013) 33-63.
- [12] K. W. Zhang; C. Banyon; C. Togbe; P. Dagaut; J. Bugler; H. J. Curran, An experimental and kinetic modeling study of n-hexane oxidation, *Combust. Flame* 162 (11) (2015) 4194-4207.
- [13] K. W. Zhang; C. Banyon; U. Burke; G. Kukkadapu; S. W. Wagnon; M. Mehl; H. J. Curran; C. K. Westbrook; W. J. Pitz, An experimental and kinetic modeling study of the oxidation of hexane isomers: Developing consistent reaction rate rules for alkanes, *Combust. Flame* 206 (2019) 123-137.
- [14] Z. D. Wang; S. M. Sarathy, Third O-2 addition reactions promote the low-temperature auto-ignition of n-alkanes, *Combust. Flame* 165 (2016) 364-372.
- [15] Z. D. Wang; B. J. Chen; K. Moshhammer; D. M. Popolan-Vaida; S. Sioud; V. S. B. Shankar; D. Vuilleumier; T. Tao; L. Ruwe; E. Brauer; N. Hansen; P. Dagaut; K. Kohse-Hoinghaus; M. A. Raji; S. M. Sarathy, n-Heptane cool flame chemistry: Unraveling intermediate species measured in a stirred reactor and motored engine, *Combust. Flame* 187 (2018) 199-216.
- [16] O. Perrin; A. Heiss; K. Sahetchian; L. Kerhoas; J. Einhorn, Determination of the isomerization rate constant $HOCH_2CH_2CH_2CH(OO \text{ center dot})CH_3 \rightarrow (HOCHCH_2CH_2CH) \cdot H \text{ center dot} (OOH)CH_3$. Importance of intramolecular hydroperoxy isomerization in tropospheric chemistry, *Int. J. Chem. Kinet.* 30 (12) (1998) 875-887.

- [17] N. Blin-Simiand; F. Jorand; K. Keller; M. Fiderer; K. Sahetchian, Ketohydroperoxides and ignition delay in internal combustion engines, *Combust. Flame* 112 (1998) 278-282.
- [18] A. Heiss; K. Sahetchian, Isomerization reactions of the n-C₄H₉O and n-OOC₄H₈OH radicals in oxygen, *Int. J. Chem. Kinet.* 28 (7) (1996) 531-544.
- [19] K. Sahetchian; J. C. Champoussin; M. Brun; N. Levy; N. Blin-Simiand; C. Aligrot; F. Jorand; M. Socoliuc; A. Heiss; N. Guerassi, Experimental study and modeling of dodecane ignition in a diesel engine, *Combust. Flame* 103 (3) (1995) 207-220.
- [20] M. Zinbo; R. K. Jensen; S. Korcek, Gas-liquid-chromatography of oxygenated compounds related to autoxidation of n-hexadecane, *Anal. Lett.* 10 (2) (1977) 119-132.
- [21] R. K. Jensen; S. Korcek; L. R. Mahoney; M. Zinbo, Liquid-phase autoxidation of organic-compounds at elevated-temperatures .1. stirred flow reactor technique and analysis of primary products from normal-hexadecane autoxidation at 120-degrees-C 180-degrees-C, *J. Am. Chem. Soc.* 101 (25) (1979) 7574-7584.
- [22] R. K. Jensen; S. Korcek; L. R. Mahoney; M. Zinbo, Liquid-phase autoxidation of organic-compounds at elevated-temperatures .2. Kinetics and mechanisms of the formation of cleavage products in normal-hexadecane autoxidation, *J. Am. Chem. Soc.* 103 (7) (1981) 1742-1749.
- [23] R. K. Jensen; M. Zinbo; S. Korcek, HPLC determination of hydroperoxidic products formed in the autoxidation of normal-hexadecane at elevated-temperatures, *J. Chromatogr. Sci.* 21 (9) (1983) 394-397.
- [24] R. K. Jensen; S. Korcek; M. Zinbo, Formation, isomerization, and cyclization reactions of hydroperoxyalkyl radicals in hexadecane autoxidation at 160-190-degrees-C, *J. Am. Chem. Soc.* 114 (20) (1992) 7742-7748.
- [25] K. Moshhammer; A. W. Jasper; D. M. Popolan-Vaida; Z. D. Wang; V. S. B. Shankar; L. Ruwe; C. A. Taatjes; P. Dagaut; N. Hansen, Quantification of the Keto-Hydroperoxide (HOOCH₂OCHO) and Other Elusive Intermediates during Low-Temperature Oxidation of Dimethyl Ether, *J. Phys. Chem. A* 120 (40) (2016) 7890-7901.
- [26] Z. Wang; L. Zhang; K. Moshhammer; D. M. Popolan-Vaida; V. S. B. Shankar; A. Lucassen; C. Hemken; C. A. Taatjes; S. R. Leone; K. Kohse-Hoinghaus; N. Hansen; P. Dagaut; S. M. Sarathy, Additional chain-branching pathways in the low-temperature oxidation of branched alkanes, *Combust. Flame* 164 (2016) 386-396.
- [27] Z. Wang; S. Y. Mohamed; L. Zhang; K. Moshhammer; D. M. Popolan-Vaida; V. S. B. Shankar; A. Lucassen; L. Ruwe; N. Hansen; P. Dagaut; S. M. Sarathy, New insights into the low-temperature oxidation of 2-methylhexane, *Proc. Combust. Inst.* 36 (1) (2017) 373-382.
- [28] Z. Wang; D. M. Popolan-Vaida; B. Chen; K. Moshhammer; S. Y. Mohamed; H. Wang; S. Sioud; M. A. Raji; K. Kohse-Hoinghaus; N. Hansen; P. Dagaut; S. R. Leone; S. M. Sarathy, Unraveling the structure and chemical mechanisms of highly oxygenated intermediates in oxidation of organic compounds, *Proceedings of the National Academy of Sciences* 114 (50) (2017) 13102-13107.
- [29] N. Belhadj; R. Benoit; P. Dagaut; M. Lailliau; Z. Serinyel; G. Dayma; F. Khaled; B. Moreau; F. Foucher, Oxidation of di-n-butyl ether: Experimental characterization of low-temperature products in JSR and RCM, *Combust. Flame* 222 (2020) 133-144.
- [30] Z. D. Wang; N. Hansen; A. W. Jasper; B. J. Chen; D. M. Popolan-Vaida; K. K. Yalamanchi; A. Najjar; P. Dagaut; S. M. Sarathy, Cool flame chemistry of diesel surrogate compounds: n-Decane, 2-methylnonane, 2,7-dimethyloctane, and n-butylcyclohexane, *Combust. Flame* 219 (2020) 384-392.
- [31] N. Belhadj; R. Benoit; P. Dagaut; M. Lailliau, Experimental characterization of n-heptane low-temperature oxidation products including keto-hydroperoxides and highly oxygenated organic molecules (HOMs), *Combust. Flame* (2021) <https://doi.org/10.1016/j.combustflame.2020.10.021>.
- [32] N. Belhadj; R. Benoit; P. Dagaut; M. Lailliau; Z. Serinyel; G. Dayma, Oxidation of di-n-propyl ether: Characterization of low-temperature products, *Proc. Combust. Inst.* 38 (1) (2021) 337-344.
- [33] N. Belhadj; R. Benoit; P. Dagaut; M. Lailliau, Experimental characterization of n-heptane low-temperature oxidation products including keto-hydroperoxides and highly oxygenated organic molecules (HOMs), *Combust. Flame* 224 (2021) 83-93.
- [34] N. Belhadj; R. Benoit; P. Dagaut; M. Lailliau, Experimental Characterization of Tetrahydrofuran Low-Temperature Oxidation Products Including Ketohydroperoxides and Highly Oxygenated Molecules, *Energy Fuels* 10.1021/acs.energyfuels.0c03291 (2021)
- [35] F. Bianchi; T. Kurtén; M. Riva; C. Mohr; M. P. Rissanen; P. Roldin; T. Berndt; J. D. Crouse; P. O. Wennberg; T. F. Mentel; J. Wildt; H. Junninen; T. Jokinen; M. Kulmala; D. R. Worsnop; J. A. Thornton; N. Donahue; H. G. Kjaergaard; M. Ehn, Highly Oxygenated Organic Molecules (HOM) from Gas-Phase Autoxidation Involving Peroxy Radicals: A Key Contributor to Atmospheric Aerosol, *Chemical Reviews* 119 (6) (2019) 3472-3509.
- [36] P. Dagaut; N. Belhadj; R. Benoit; G. Dayma; M. Lailliau; Z. Serinyel, in: *MCS11 11th Mediterranean Combustion Symposium* <https://hal.archives-ouvertes.fr/hal-02137413>, Tenerife, Spain, 2019.
- [37] P. Dagaut; M. Cathonnet; J. P. Rouan; R. Foulatier; A. Quilgars; J. C. Boettner; F. Gaillard; H. James, A Jet-Stirred Reactor for Kinetic-Studies of Homogeneous Gas-Phase Reactions at Pressures up to 10-Atmospheres (~ 1 MPa), *Journal of Physics E-Scientific Instruments* 19 (3) (1986) 207-209.
- [38] A. El Bakali; P. Dagaut; L. Pillier; P. Desgroux; J. F. Pauwels; A. Rida; P. Meunier, Experimental and modeling study of the oxidation of natural gas in a premixed flame, shock tube, and jet-stirred reactor, *Combust. Flame* 137 (1-2) (2004) 109-128.
- [39] T. Le Cong; P. Dagaut, Experimental and Detailed Modeling Study of the Effect of Water Vapor on the Kinetics of Combustion of Hydrogen and Natural Gas, Impact on NO_x, *Energy Fuels* 23 (1) (2009) 725-734.

- [40] A. Ristori; P. Dagaut; M. Cathonnet, The oxidation of n-hexadecane: Experimental and detailed kinetic modeling, *Combust. Flame* 125 (3) (2001) 1128-1137.
- [41] S. Thion; C. Togbe; Z. Serinyel; G. Dayma; P. Dagaut, A chemical kinetic study of the oxidation of dibutyl-ether in a jet-stirred reactor, *Combust. Flame* 185 (2017) 4-15.
- [42] R. Benoit; N. Belhadj; M. Lailliau; P. Dagaut, On the similarities and differences between the products of oxidation of hydrocarbons under simulated atmospheric conditions and cool-flames, *Atmos. Chem. Phys. Discuss.* 2020 (2020) <https://doi.org/10.5194/acp-2020-1070>.
- [43] N. Belhadj; R. Benoit; P. Dagaut; M. Lailliau, Experimental Characterization of Tetrahydrofuran Low-Temperature Oxidation Products Including Ketohydroperoxides and Highly Oxygenated Molecules, *Energy Fuels* 35 (9) (2021) 7242–7252.
- [44] N. Belhadj; R. Benoit; P. Dagaut; M. Lailliau; B. Moreau; F. Foucher, Low-temperature oxidation of a gasoline surrogate: Experimental investigation in JSR and RCM using high-resolution mass spectrometry, *Combust. Flame* 228 (2021) 128-141.
- [45] R. Benoit; N. Belhadj; M. Lailliau; P. Dagaut, On the similarities and differences between the products of oxidation of hydrocarbons under simulated atmospheric conditions and cool flames, *Atmos. Chem. Phys.* 21 (10) (2021) 7845-7862.
- [46] P. Glarborg; R. J. Kee; J. F. Grcar; J. A. Miller in: *PSR: A FORTRAN program for modeling well-stirred reactors.*, SAND86-8209, Sandia National Laboratories, Livermore, CA, 1986
- [47] R. J. Kee; F. M. Rupley; J. A. Miller in: *CHEMKIN-II: A Fortran Chemical Kinetics Package for the Analysis of Gas-Phase Chemical Kinetics.*, SAND89-8009, Sandia National Laboratories, Livermore, CA, 1989
- [48] A. Rodriguez. Combustion study of organic compounds by coupling a jet-stirred reactor with spectroscopic and spectrometric analytical methods : application to the detection of hydroperoxides. Étude de la combustion de composés organiques grâce au couplage d'un réacteur parfaitement agité avec des méthodes analytiques spectroscopiques et spectrométriques : application à la détection des hydroperoxydes. Ph.D. Thesis, Université de Lorraine, Nancy, France, 2016.
- [49] O. Herbinet; B. Husson; Z. Serinyel; M. Cord; V. Warth; R. Fournet; P. A. Glaude; B. Sirjean; F. Battin-Leclerc; Z. D. Wang; M. F. Xie; Z. J. Cheng; F. Qi, Experimental and modeling investigation of the low-temperature oxidation of n-heptane, *Combust. Flame* 159 (12) (2012) 3455-3471.
- [50] A. Jalan; I. M. Alecu; R. Meana-Paneda; J. Aguilera-Iparraguirre; K. R. Yang; S. S. Merchant; D. G. Truhlar; W. H. Green, New Pathways for Formation of Acids and Carbonyl Products in Low-Temperature Oxidation: The Korcek Decomposition of gamma-Ketohydroperoxides, *J. Am. Chem. Soc.* 135 (30) (2013) 11100-11114.
- [51] C. A. Grambow; A. Jamal; Y. P. Li; W. H. Green; J. Zador; Y. V. Suleimanov, Unimolecular Reaction Pathways of a gamma-Ketohydroperoxide from Combined Application of Automated Reaction Discovery Methods, *J. Am. Chem. Soc.* 140 (3) (2018) 1035-1048.
- [52] N. Blin-Simiand; F. Jorand; K. Sahetchian; M. Brun; L. Kerhoas; C. Malosse; J. Einhorn, Hydroperoxides with zero, one, two or more carbonyl groups formed during the oxidation of n-dodecane, *Combust. Flame* 126 (1) (2001) 1524-1532.
- [53] M. Pelucchi; M. Bissoli; C. Cavallotti; A. Cuoci; T. Faravelli; A. Frassoldati; E. Ranzi; A. Stagni, Improved Kinetic Model of the Low-Temperature Oxidation of n-Heptane, *Energy Fuels* 28 (11) (2014) 7178-7193.
- [54] R. H. West; C. F. Goldsmith, The impact of roaming radicals on the combustion properties of transportation fuels, *Combust. Flame* 194 (2018) 387-395.
- [55] A. J. Eskola; I. O. Antonov; L. Sheps; J. D. Savee; D. L. Osborn; C. A. Taatjes, Time-resolved measurements of product formation in the low-temperature (550-675 K) oxidation of neopentane: a probe to investigate chain-branching mechanism, *Phys. Chem. Chem. Phys.* 21 (2017) 13731-13745.